Combining Copula Theory and Machine Learning for Prediction of Ground Vibrations Induced by Tunnel Blasting

Yawen Cao[1,2], Rui Ma[3,*], Leifeng Zhang[4], Xiaofei Du[1], Wenjin Liu[1] and Qixiang Gao[1]

[1] North China Engineering Investigation Institute Co., Ltd., Shijiazhuang, 050021, China

[2] Technology Innovation Center for Groundwater Disaster Prevention and Control Engineering for Metal Mines, Ministry of Natural Resources, Shijiazhuang, 050021, China

[3] School of Software, Hefei University of Technology, Hefei, 230601, China

[4] College of Architecture and Civil Engineering, Beijing University of Technology, Beijing, 100124, China

INFORMATION

Keywords:
Blast vibration
peak particle velocity
Copula theory
dependence modeling
coupled prediction model

DOI: 10.23967/j.rimni.2025.10.72042

SCIPEDIA Revista Internacional de Métodos Numéricos para Cálculo y Diseño en Ingeniería

Revista Internacional Métodos numéricos para cálculo y diseño en ingeniería RIMNI in cooperation with CIMNE

Combining Copula Theory and Machine Learning for Prediction of Ground Vibrations Induced by Tunnel Blasting

Yawen Cao[1,2], Rui Ma[3,*], Leifeng Zhang[4], Xiaofei Du[1], Wenjin Liu[1] and Qixiang Gao[1]

[1]North China Engineering Investigation Institute Co., Ltd., Shijiazhuang, 050021, China

[2]Technology Innovation Center for Groundwater Disaster Prevention and Control Engineering for Metal Mines, Ministry of Natural Resources, Shijiazhuang, 050021, China

[3]School of Software, Hefei University of Technology, Hefei, 230601, China

[4]College of Architecture and Civil Engineering, Beijing University of Technology, Beijing, 100124, China

ABSTRACT

To effectively predict and control the peak particle velocity (PPV) induced by tunnel blasting, this study investigates the Qinhuangdao Jiaoshan Tunnel as a case study. This study first proposes an Improved Particle Swarm Optimization (IPSO) algorithm through theoretical derivation. Building upon IPSO, a further enhanced algorithm, termed CIPSO, is developed by integrating a dependency model derived from Copula theory. The CIPSO algorithm is then employed to optimize a Support Vector Regression (SVR) model, establishing the final CIPSO-SVR prediction framework. Copula theory was employed to quantify the correlation between PPV and surface cumulative settlement (S). A regularization term incorporating Kullback-Leibler (KL) divergence was then embedded into the SVR objective function. The Hyperparameters of the CIPSO-SVR model were optimized using fixed-step rolling cross-validation. The model's predictive performance was rigorously compared against CIPSO-optimized Convolutional Neural Network (CNN) and Long Short-Term Memory (LSTM) models, as well as against SVR, CNN, and LSTM models optimized by the Grey Wolf Optimizer (GWO) and Moth-Flame Optimization (MFO) algorithms. The results show that the CIPSO-SVR model achieves superior accuracy and robustness on the test set ($R^2 = 0.9569$) in predicting PPV compared to the alternative models. Crucially, the model effectively captures the inherent nonlinear relationships of complex engineering problems, even with small-sample data.

OPEN ACCESS

Received: 18/08/2025

Accepted: 17/10/2025

Published: 23/01/2026

DOI
10.23967/j.rimni.2025.10.72042

Keywords:
Blast vibration
peak particle velocity
Copula theory
dependence modeling
coupled prediction model

1 Introduction

Blasting is one of the most commonly used methods for tunnel construction. However, it generates stress waves that can reduce the mechanical properties of the surrounding rock mass, compromise its stability [1], and thus pose a threat to nearby structures [2]. The PPV induced by blasting is a key metric for assessing its impact on adjacent buildings and structures [3,4]. Consequently, the accurate prediction of PPV is essential for ensuring project safety [5]. Currently, the primary approaches for

*Correspondence: Rui Ma (mr091111@163.com).

PPV prediction include empirical formulas, fuzzy inference systems, and machine learning techniques, among others.

The formulaic approach relies on the regression and empirical fitting of extensive field data. However, in practice, factors like the internal interactions within the rock and soil mass significantly limit its predictive accuracy for PPV. As a result, substantial deviations often occur between predictions and measured data [6].

To address these limitations, numerous studies have proposed new empirical methodshave been proposed. For instance, Deng et al. [7] derived an attenuation formula for elastic stress wave propagation based on stress wave theory, which was subsequently corrected for multi-hole, multi-stage blasting conditions. Field validation demonstrated that the modified formula achieves PPV prediction with low relative error. Luo et al. [8] noted that the distribution of PPV in deep underground spaces differs from that on the surface, finding Sadovsky's formula inadequate for such environments. To tackle this issue, they employed a method combining field measurements, numerical simulation, mechanical analysis and dimensional analysis to derive a new PPV prediction formula for cavern sidewalls. Comparisons with field data, Sadovsky's formula, and simulation results confirmed the superior performance of their formula in deep underground settings. Separately, Tribe et al. [9] introduced a novel PPV formula based on quantile-based analysis (DA), integrating key blast design parameters. Their model was field-validated, achieved a high R^2 and had the lowest MAE values.

Fuzzy inference systems have also been widely applied to PPV prediction. For example, Chen et al. [10] introduced a method based on the Mamdani fuzzy inference system. This approach first employs minimum redundancy maximum correlation to identify key blast design parameters influencing PPV, then uses K-means clustering to determine their value ranges. These parameters and ranges are subsequently input into the Mamdani system for prediction, with field data confirming the model's superior performance. In a separate study, Ghasemi et al. [11] combined an Adaptive Neuro-Fuzzy Inference System (ANFIS) with PSO to predict PPV in open-pit mines. The accuracy of this ANFIS-PSO model was validated through favorable comparisons with USBM empirical equations.

Recent advances in computer technology have enabled the widespread adoption of deep learning for predictive models in engineering [12,13]. Driven by this trend, research in PPV prediction has increasingly focused on hybridizing different models to enhance accuracy, with promising results [14–16].

Although machine learning models have improved PPV prediction to some extent, there are still some problems. Traditional machine learning methods often struggle with large-scale datasets, while deep learning approaches can be hampered by training difficulties and high computational costs [17]. To address these issues, this study proposes a novel method that integrates Copula theory into a deep learning framework by capitalizing on the correlation between PPV and S. Copula theory provides a well-established means of characterize dependence between variables [18,19]. Consequently, the first step of our methodology involves constructing a Copula model to identify the function that best describes the PPV-S correlation. Subsequently, a theoretically enhanced PSO algorithm is employed to optimize an SVR model. Finally, the dependence structure captured by the Copula model is embedded into the machine learning objective function as the regularization term using the KL divergence. This constraint forces the model's predictions to adhere to the statistical correlation between PPV and S., enabling accurate prediction even with limited samples and thereby facilitating the proactive mitigation of potential accidents. The novelty and niche of this study are highlighted in the following aspects:

Novelty:

1) A key novelty of this work lies in the application of Copula theory to precisely characterize the complex, non-linear interdependence between Peak Particle Velocity (PPV) and surface settlement (S) during tunnel blasting. By constructing a Gumbel Copula model, we identified a significant positive correlation and, more importantly, a strong upper-tail dependence between these two parameters. This finding indicates that the probability of observing substantial settlement increases non-linearly when blast-induced vibration intensifies to extreme levels. In other words, under conditions approaching the safety threshold, PPV and S exhibit an amplified, coordinated response rather than varying independently.

2) Furthermore, we integrate this quantitatively established dependence as a physical constraint into the learning process of the Support Vector Regression (SVR) model. This is achieved by incorporating a Kullback-Leibler (KL) divergence-based regularization term into the SVR's loss function. Consequently, during training, the CIPSO-SVR model is optimized not only for predictive accuracy but also for ensuring its outputs adhere to the discovered physical relationship between PPV and S.

Niche

1) The model is specifically designed for challenging engineering scenarios where data is expensive or difficult to obtain. In such contexts, standard deep learning models are prone to overfitting, and traditional empirical methods are not accurate enough. Our method provides a robust solution tailored to these constraints.

2) A key advantage of our model over conventional machine learning is the physical consistency constraint introduced via the KL divergence term. This ensures the predictions are not only accurate but also physically plausible, which fosters greater trust and acceptance among field engineers, thereby significantly promoting their practical adoption.

2 Background

The Jiao Shan Tunnel is a component of the National Highway G102 improvement project in Qinhuangdao City, situated in the Jiao Shan area of Shanhaiguan District. Given that the tunnel passes beneath the Great Wall, strict control of deformation and blasting vibration is paramount. In this study, five monitoring sections (S1–S5) were established 100 m west of the Great Wall, spaced 10 m i apart. Each section contained eleven monitoring points (D1–D11) installed at 5 m intervals, with point D6 aligned with the tunnel centerline. The layout plan and longitudinal section are provided in Figs. 1 and 2, respectively.

Vibration data generated during blasting operations were recorded using a Donghua DH5908N vibration acquisition instrument, coupled with magnetoelectric vibration sensors. The sensitivity of the sensors was 0.3 V/(m/s). The data acquisition system was configured with a sampling frequency of 100 kHz and incorporated a built-in 1–500 Hz band-pass filter to suppress high-frequency noise and low-frequency interference. The system exhibits a dynamic range greater than 100 dB and an overall measurement accuracy of 1%. Annual calibration was performed by an accredited metrology laboratory to ensure measurement traceability.

The peak particle velocity (PPV) was derived from the three-channel data (vertical, radial, and tangential) using the vector synthesis method:

$$PPV = \sqrt{PPV_x^2 + PPV_y^2 + PPV_z^2} \tag{1}$$

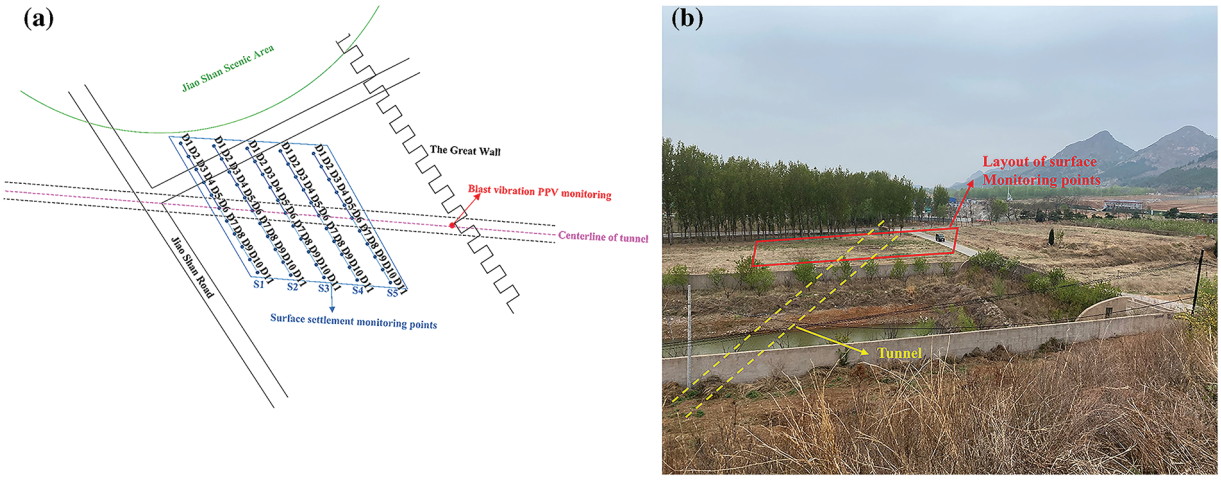

Figure 1: Layout plan of the monitoring system at the Jiao Shan Tunnel site. Five monitoring sections (S1–S5) are spaced 10 m apart, each containing eleven monitoring points (D1–D11) at 5 m intervals. Point D6 is aligned with the tunnel centerline, which is the focus of subsequent correlation and modeling analysis (a, b). The tunnel was excavated using gas-generating devices for pre-splitting, with the working face divided into three parts: the upper portion of the upper, the lower portion of upper bench and the lower bench. The blast hole arrangement is illustrated in Fig. 2. Since the settlement data were collected following vibrations induced by the lower bench excavation, this study specifically focuses on the lower bench excavation parameters for analysis

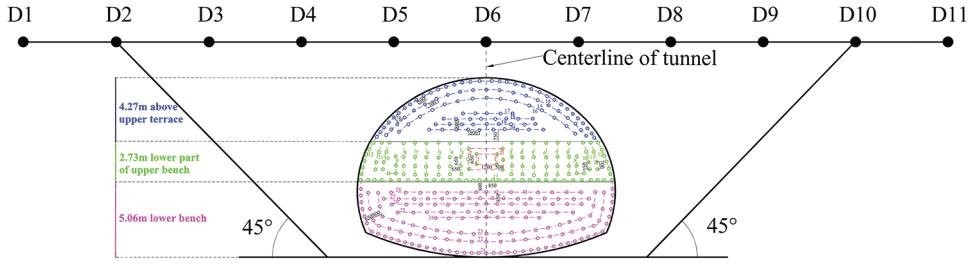

Figure 2: Longitudinal profile illustrating the settlement monitoring points and the blast hole layout. The settlement data analyzed in this study were specifically collected during the blasting operations of the lower bench, hence the focus on its excavation parameters

The unit for Peak Particle Velocity (PPV) throughout this study is centimeters per second (cm/s). Outliers were identified and removed based on two criteria: (a) data records showing clear signs of sensor failure, such as signal saturation or loss of connection; and (b) records where the measured PPV fell outside the range of ±3 standard deviations from the value estimated by the Sadovsky empirical formula. Furthermore, the dominant frequency (F), which was extracted from the vibration signal using Fast Fourier Transform (FFT) analysis, served as an input feature for the prediction model.

Settlement data collected from the five sections during identical blasting periods, yielding a total of 25 datasets. After the exclusion of outliers, 23 datasets remained. These were subsequently partitioned into training and testing sets with an 80:20 ratio, the first 80% of the data were used for training, and the remaining 20% were reserved for testing. The corresponding settlement curve is presented in Fig. 3.

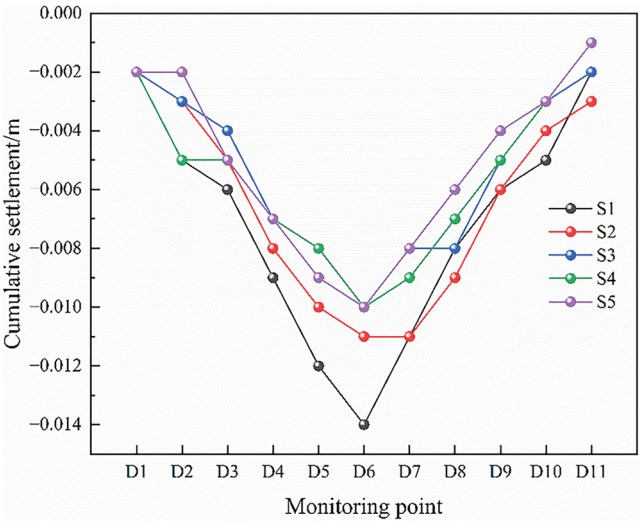

Figure 3: Cumulative settlement curves for each section and each monitoring point

According to Fig. 3, it can be seen that the surface settlement distribution across all sections approximates an orthogonal distribution, with the maximum settlement consistently located at the tunnel centerline. Specifically, section S1 exhibits the greatest settlement at its centerline. As Fig. 1 shows, both monitoring point D6 and the blasting vibration monitoring points are aligned with the tunnel centerline, and the settlement at D6 is indeed the largest. This typical behavior justifies the focus of this study on point D6 within section S1.

Blast vibration data were collected concurrently, digitized by the data acquisition system, and simultaneously transmitted to the data processing center and control system via a dedicated protocol. The data were then relayed to the field engineer via the Internet. The relationship between PPV and settlement at point D6 is shown in Fig. 4.

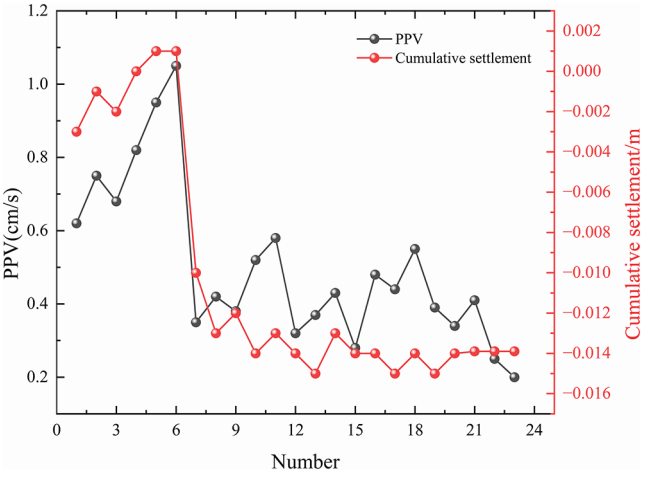

Figure 4: PPV vs. D6 settlement curves

Fig. 4 reveals a clear positive correlation between PPV and S, where larger settlements correspond to stronger vibrations. Therefore, when building a prediction model, the correlation between parameters can be considered to improve the prediction performance of the model. The S correlation between PPV and D6 is modeled by Copula theory to find a suitable Copula theory model for the Jiao Shan Tunnel.

3 Research Methodology

3.1 Copula Theory

Copula theory, first proposed by Sklar [20] in 1959, is a widely used statistical tool for characterizing dependence structures among random variables. Consider random variables $X_1,\ X_2, \ldots,\ X_N$ with joint distribution function $F\left(X_1,\ X_2, \cdots,\ X_N\right)$ and marginal distribution function $U_1 = F_1\left(X_1\right),\ U_2 = F_2\left(X_2\right), \cdots,\ U_N = F_N\left(X_N\right)$. Sklar's theorem states that there exists a function $C\left(U_1,\ U_2, \cdots,\ U_N\right)$, called a Copula, such that the joint distribution can be expressed as:

$$F\left(X_1,\ X_2, \cdots,\ X_N\right) = C\left(F_1\left(X_1\right),\ F_2\left(X_2\right), \cdots,\ F_N\left(X_N\right)\right) = C\left(U_1,\ U_2, \ldots,\ U_N\right) \tag{2}$$

The Archimedean Copula function expression is [21,22]:

$$C\left(U_1, U_2, \ldots, U_N; \varphi_\theta\right) = \varphi_\theta^{-1}\left(\varphi_\theta\left(U_1\right) + \varphi_\theta\left(U_2\right) + \cdots + \varphi_\theta\left(U_N\right)\right) \tag{3}$$

where θ is the parameter; $\varphi_\theta\left(\cdot\right)$ is the generator function; $\varphi_\theta^{-1}\left(\cdot\right)$ is its inverse.

Copula functions mainly include elliptic function clusters and Archimedean function clusters, and elliptic function clusters include Gaussian, t, while Archimedean function clusters include Frank, Clayton, Gumbel. This study evaluates these five candidate functions to identify the most suitable one for modeling dependencies in the Jiao Shan Tunnel project.

The optimal Copula function is selected using the Akaike Information Criterion (AIC) and Bayesian Information Criterion (BIC), where lower values indicate a better model fit [23].

$$AIC = 2i - 2\ln\left(L\right) \tag{4}$$

$$BIC = \ln\left(N\right) i - 2\ln\left(L\right) \tag{5}$$

where i is the number of parameters, N is the sample size, L is the maximum likelihood function.

The optimal Copula function is selected by computing the corresponding AIC and BIC values for each candidate using Eqs. (4) and (5). Furthermore, as indicated in Section 4.1, a certain positive correlation exists between PPV and settlement, which suggests potential upper tail dependence. To quantitatively describe the correlation under extreme variable values, this study employs tail dependence coefficients. The upper and lower tail dependence coefficients, denoted as λ_U and λ_L, respectively, are defined in Eqs. (6) and (7) [24].

$$\lambda_U = \lim_{q \to 1} P\left[X \geq \mathrm{F}_X^{-1}\left(q\right) \middle| Y \geq \mathrm{F}_Y^{-1}\left(q\right)\right] \tag{6}$$

$$\lambda_L = \lim_{q \to 0} P\left[X < F_X^{-1}\left(q\right) \middle| Y < F_Y^{-1}\left(q\right)\right] \tag{7}$$

where X and Y are random variables, q is a random probability value from 0 to 1, F_X, F_Y are the marginal distribution function of X and Y, respectively, $F_X^{-1}\left(q\right)$ and $F_Y^{-1}\left(q\right)$ are the quantile function of X and Y, respectively, and P is the probability function.

When $\lambda_U = 0$ or $\lambda_L = 0$, the variables are independent under extremely high or low values, respectively. When $\lambda_U = 1$ or $\lambda_L = 1$, the variables exhibit perfect co-movement under the

corresponding extremes; When $0 < \lambda_U < 1$ or $0 < \lambda_L < 1$, it indicates a positive correlation under extremes, with the strength of dependence increasing with the value of the coefficient [25].

To facilitate a clearer comparison of the differences between the Copula functions, simulations were conducted using the five candidate functions. Fig. 5 illustrates the simulation results for each function alongside radar charts of their AIC and BIC values. The corresponding tail dependence coefficients, λ_U and λ_L values are shown in Table 1.

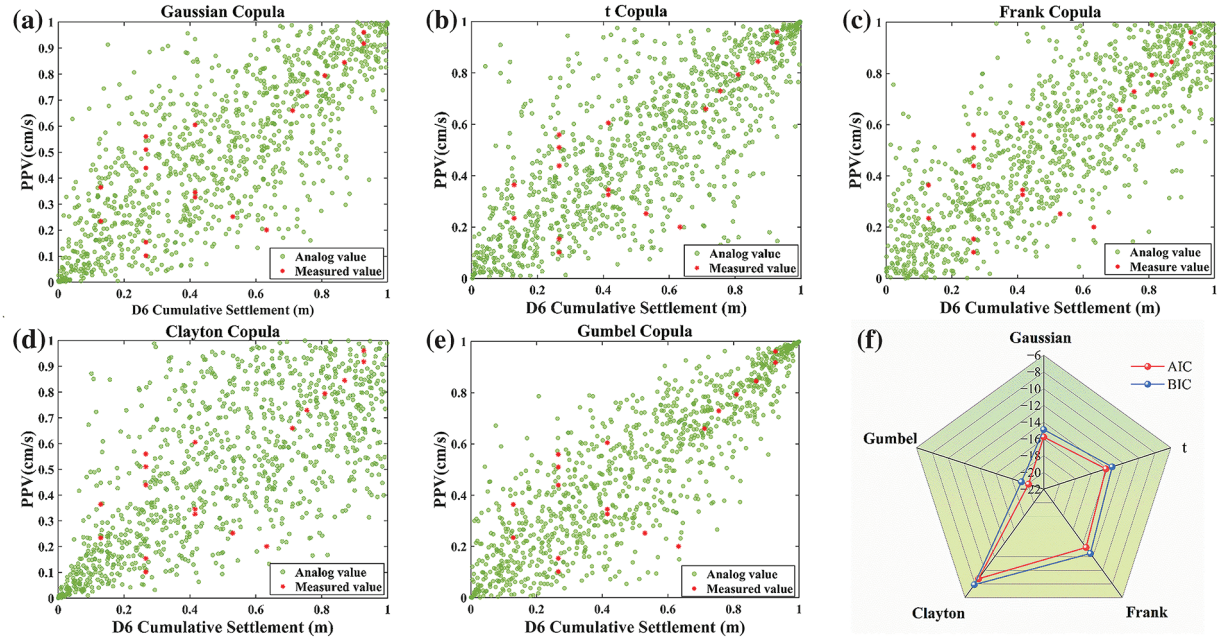

Figure 5: Comparison of Copula functions for modeling the dependence between PPV and settlement (S): **(a)** Scatter plots of simulated data from Gaussian Copula functions; **(b)** Scatter plots of simulated data from t Copula functions; **(c)** Scatter plots of simulated data from Frank Copula functions; **(d)** Scatter plots of simulated data from Clayton Copula functions; **(e)** Scatter plots of simulated data from Gumbel Copula functions; **(f)** Radar chart comparing the Akaike (AIC) and Bayesian (BIC) information criteria for each function; lower values indicate a better fit. The Gumbel Copula demonstrates the lowest AIC/BIC values and its simulated data (**c**) best capture the upper-tail dependence (high PPV with high settlement) observed in the actual data, making it the most suitable model

Table 1: Tail dependence coefficients corresponding to different functions

Dependence on the tail	Gaussian	t	Frank	Clayton	Gumbel
λ_U	0.0000	0.4947	0.0000	0.0000	0.7417
λ_L	0.0000	0.4947	0.0000	0.7035	0.0000

The selection of the optimal Copula function is based on AIC/BIC criteria and tail dependence analysis, as summarized in Fig. 5 and Table 1. Fig. 5f clearly shows that the Gumbel Copula yields the lowest AIC and BIC values, indicating the best statistical fit. More importantly, the scatter plot of

the Gumbel Copula (Fig. 5c) shows a higher density of points in the upper-right quadrant (high PPV, high settlement), which visually confirms its ability to capture the upper-tail dependence ($\lambda_U = 0.7417$, Table 1). This characteristic aligns with the physical intuition that strong vibrations are associated with significant settlements. Therefore, the Gumbel Copula is selected to quantify the PPV-S correlation.

3.2 Modeling of Blasting Vibration and Surface Settlement

3.2.1 SVR Principles

SVR was proposed by Vapnik et al. [26] in 1997, is suitable for modeling and identifying nonlinear, small-sample, and high-dimensional problems [27]. The core objective of SVR is to find a function$f(x) = k\phi(X) + b$ that maps input data to a high-dimensional feature space via the function $\phi(X)$. The Radial Basis Function (RBF) was selected as the kernel function for this study.

3.2.2 Improved Particle Swarm Optimization (IPSO) Algorithm

Particle swarm optimization was proposed by Kennedy and Eberhart in 1995, and is a heuristic global optimization algorithm inspired by the social behavior of animals warms. The goal of the PSO algorithm optimization is to find the parameters of the best objective function in the search space. In this algorithm, each particle represents a potential solution within the search space. The algorithm iteratively updates each particle's velocity and position based on its own historical best position (P_{best}), and the swarm's global best position (G_{best}), guiding the population toward the optimal. Assuming that the total number of particles in the N-dimensional space is D, the update equations for the positions and velocities of the particles are shown below [28].

$$x_{ij}(t+1) = x_{ij}(t) + v_{ij}(t+1) \tag{8}$$

$$v_{ij}(t+1) = \omega v_{ij}(t) + c_1 r_1(t)\left(P_{best} - x_{ij}(t)\right) + c_2 r_2(t)\left(G_{best} - x_{ij}(t)\right) \tag{9}$$

where $i = 1, 2, 3,\ldots,$ N and $j = 1, 2,\ldots,$ D. N is the total number of particle in the swarms and D is the dimensionality of the search space. The parameter ω is the inertia weight; x_{ij} and v_{ij} represent the position and velocity components of the i-th particle in the j-th dimension, respectively; c_1 and c_2 are the learning factors; r_1 and r_2 are random numbers uniformly distributed in the range [0, 1]; P_{best} is the best position of the i-th particle at time t; and G_{best} is the global best position of the i-th particle in the overall.

The standard Particle Swarm Optimization (PSO) algorithm can suffer from slow convergence and a tendency to become trapped in local optima when dealing with complex problems. To address these limitations, an Improved PSO (IPSO) is proposed. A key modification involves simplifying the position update by removing the direct influence of the velocity term, leading to the following update equation:

$$x_{ij}(t+1) = \frac{c_1 r_1(t)\left(P_{best} - x_{ij}(t)\right) + c_2 r_2(t)\left(G_{best} - x_{ij}(t)\right)}{(1-\omega)} \tag{10}$$

A comparison of the convergence performance between the standard PSO and the Improved PSO (IPSO) algorithms is presented in Fig. 6.

As shown in Fig. 6, the fitness value of the IPSO algorithm converges after 50 iterations, whereas the PSO algorithm requires approximately 60 generations to stabilize. Moreover, the converged fitness value achieved by IPSO is lower than that of PSO, demonstrating its faster convergence rate and superior accuracy in addressing complex nonlinear engineering problems.

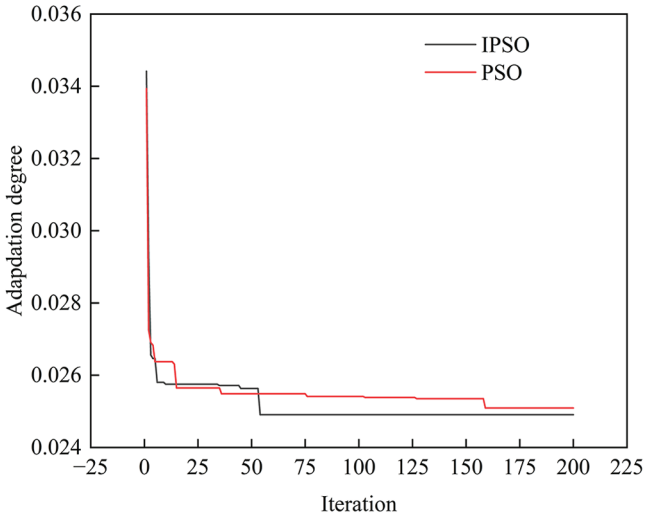

Figure 6: Convergence performance comparison between the standard PSO and the proposed Improved PSO (IPSO) algorithms

3.2.3 Modeling of CIPSO-SVR Coupling

Suppose: X is the S, Y is the PPV, x and y are arbitrary real numbers, and the marginal distribution function is shown below:

$$u = F_X(x) = P\{X \le x\}, v = F_Y(y) = P\{Y \le y\} \tag{11}$$

According to Section 4.2, it is known that the Gumbel function can better express the correlation between S and PPV, so the joint distribution function is [29]:

$$C_\theta(u, v) = \exp\left[-\left((-\ln u)^\theta + (-\ln v)^\theta\right)^{\frac{1}{\theta}}\right] \tag{12}$$

The corresponding Copula density function is [30]:

$$\frac{\partial^2 C}{\partial u \partial v} = C_\theta(u, v) \cdot \frac{[(-\ln u)(-\ln v)]^{\theta-1}}{uv} \cdot \left[1 + (\theta - 1)\left((-\ln u)^\theta + (-\ln v)^\theta\right)^{-\frac{1}{\theta}}\right] \tag{13}$$

where θ is the basic parameter that determines the Copula function.

The Copula conditional probability density function of PPV on S is:

$$p_c = \frac{\partial^2}{\partial u \partial v} C(u, v) \cdot f_Y(y) \tag{14}$$

where $f_Y(y)$ is the edge probability density function of the PPV.

The difference between the predictive distribution of the model and the distribution of the true values is quantified by the KL divergence, and the KL definition formula is shown as follows [31]:

$$KL(p_m \parallel p_c) = \int p_m(x) \log \frac{p_m(x)}{p_c(x)} dx \tag{15}$$

Monte Carlo approximation:

$$KL \approx \frac{1}{N}\sum_{i=1}^{N}\log\frac{p_m(x)}{p_c(x)} \tag{16}$$

where N is the number of samples.

Eq. (16) is added to the SVR objective function so that the model predicted distribution obeys the Copula-theoretic dependence of the PPV on the S, as shown in the following equation:

$$\min_{\omega,b,\xi}\frac{1}{2}\|\omega\|^2 + c\sum_{i=1}^{N}\left(\xi_i+\xi_i^*\right)+\eta KL \tag{17}$$

where η is the weight factor of the constraint term ($\eta > 0$) which was optimized alongside other hyperparameters via cross-validation. When η is relatively large, the model tends to prioritize the Copula theory constraints. Conversely, an excessively small η value leads the model to focus primarily on error minimization in traditional SVR, potentially neglecting the physical constraints.

The introduced regularization term provides more than a mathematical constraint; it enhances model generalizability and physical consistency. This term first serves as a strong physical inductive bias. Under small-sample conditions, it mitigates overfitting and unreasonable predictions for new data by ensuring outputs align with the learned PPV-S dependence. This significantly improves the model's generalization capability and practical reliability. Second, from a blasting dynamics viewpoint, it acts as an energy consistency constraint. The upper-tail dependence identified by the Gumbel Copula reflects the nonlinear correlation between intense vibration (high PPV) and substantial deformation (large S), rooted in energy transfer. This regularization guarantees that the predictions are not only consistent with the data but also comply with this fundamental energy principle, ensuring physical plausibility.

The CIPSO-SVR flowchart is shown in Fig. 7.

To evaluate the performance of the CIPSO-SVR model in small samples PPV prediction, the CIPSO and IPSO algorithms were configured with identical parameter values. Both models were trained and tested on the field measured dataset. The prediction errors (PPV (Predicted value-True value)) for both models are presented using box plots in Fig. 8 to determine the performance of SVR models optimized by the CIPSO and IPSO algorithms, respectively.

As shown in Fig. 8, the box plot for CIPSO-SVR is narrower than that of IPSO-SVR, demonstrating a more concentrated distribution of prediction errors. the CIPSO-SVR results contain no outliers, whereas two outliers are present in the IPSO-SVR results. This suggests that CIPSO-SVR relies on the correlation between PPV and S correlation to align the predictions more closely with actual values.

3.2.4 PPV and Surface Settlement Modeling

The model incorporates four main parameters: cumulative settlement (S), maximum charge per delay (Q), blast center distance (R), and frequency (F). The parameter S is employed solely during the initial modeling phase, where Copula theory is applied to identify a function that accurately captures the nonlinear dependence between S and PPV. In the subsequent phase, an Improved Particle Swarm Optimization-based Support Vector Regression (IPSO-SVR) model is constructed, integrating the previously determined Copula function into the SVR objective function. This leads to the proposed CIPSO-SVR model, which accepts Q, R, and F as inputs and outputs the predicted PPV. The KL scatter constructs regularization terms embedded in the SVR objective function so that the model

can predict values closer to the true values under small sample conditions. In order to demonstrate the performance of the CIPSO algorithm, two optimization algorithms, GWO and MFO, are used as comparisons. Using these three algorithms coupled with three prediction models, SVR, CNN and LSTM, respectively. The range of parameter values for each prediction model and optimization algorithm are shown in Tables 2 and 3.

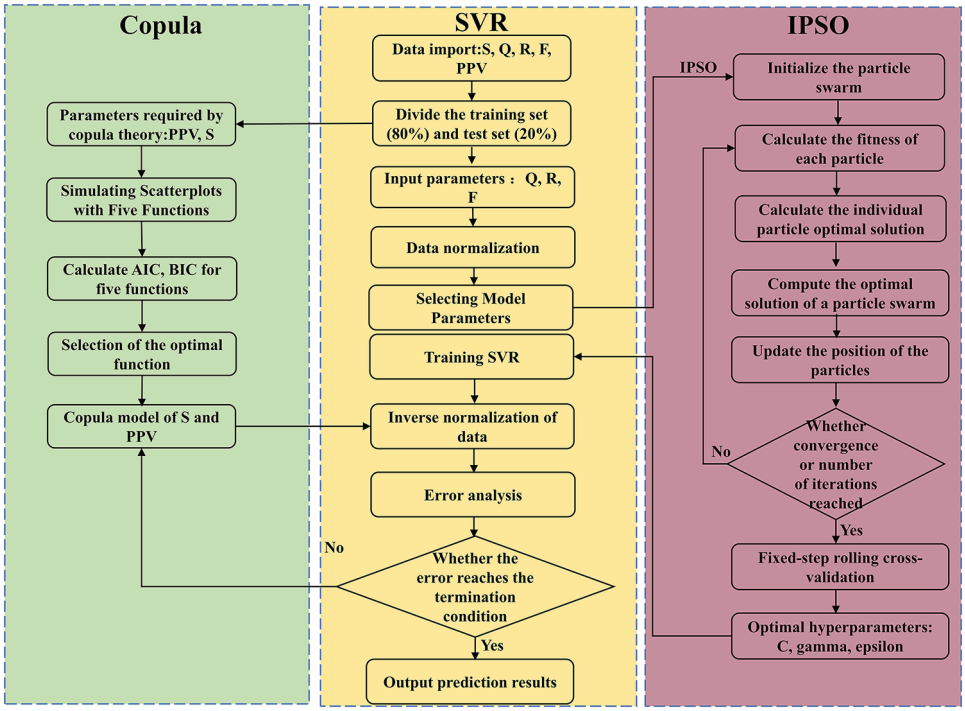

Figure 7: CIPSO-SVR flowchart

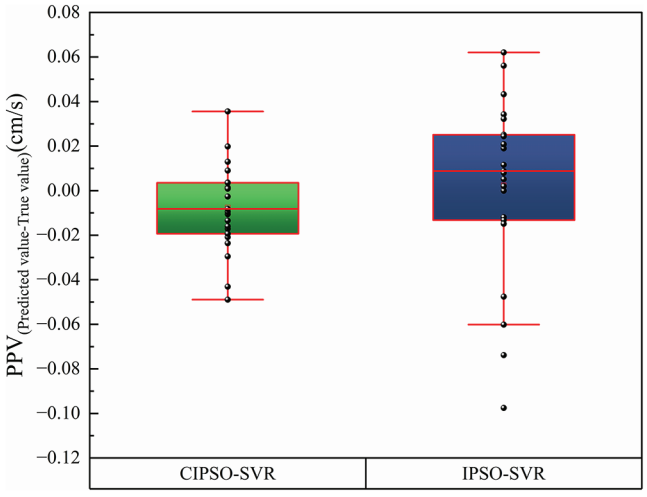

Figure 8: Prediction error comparison of SVR models optimized by the IPSO and the CIPSO algorithms

Table 2: Range of values for each model parameter

Prediction model	Key parameters	Value range
SVR	Regularization parameter-C	[0.1, 100]
	Gamma	[0.001, 100]
	Epsilon	[0.01, 100]
	η_1	$(0, +\infty)$
CNN	FilterSize	[1, 10]
	NumFilters	[5, 100]
	η_2	$(0, +\infty)$
LSTM	Number of hidden units	[10, 1000]
	Learning rate	[0.0001, 0.1]
	Dropout rate	[0, 0.5]
	η_3	$(0, +\infty)$

Table 3: Parameter settings for the three optimization algorithms

Algorithm type	Parameters	Values
CIPSO	Population size	10
	Number of iterations	50
	C1	1.75
	C2	1.75
	wmax	0.9
	wmin	0.4
GWO	Population size	10
	Number of iterations	50
MFO	Population size	10
	Number of iterations	50

The particle swarm optimization algorithm requires strong global exploration capabilities at the initial stage and refined local exploitation capabilities near convergence. To balance this trade-off, a time-varying inertia weight ω is introduced [32], which decreases as the iteration count increases.

$$\omega = \omega_{\max} - (\omega_{\max} - \omega_{\min}) \times \frac{i}{T_{\max}} \tag{18}$$

where $\omega_{\max}$ is the maximum inertial weight, set to 0.9; $\omega_{\min}$ is the minimum inertial weight, set to 0.4; $T_{\max}$ is the maximum iteration count; i is the current iteration count.

3.2.5 Cross-Validation Hyperparameter Optimization

This study employed a fixed-step rolling cross-validation [33] approach to verify model robustness and determine the optimal hyperparameters. To prevent data leakage, the entire cross-validation

process was strictly confined to the training dataset, while the test set was reserved exclusively for the final performance evaluation. This is done The specific process was as follows: G1–G13 were used for the training, set and validated on G14; subsequently, group 2–14 were used for the training, set and validated on group 15; as the validation set; group 3–15 as thewere used for training, set and validated on group 16; as the validation set, and is the entire process was repeated for a total of five times in total rounds. The specific flowchart is shown in Fig. 9.

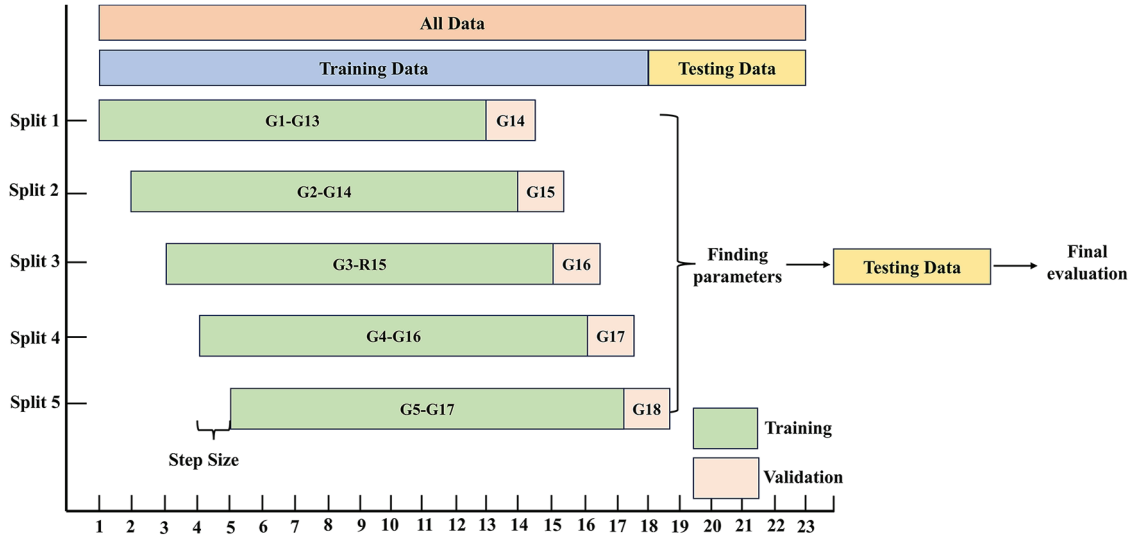

Figure 9: Schematic of the model development and evaluation workflow. The model was developed using a two-stage process. A fixed-step rolling cross-validation was conducted exclusively on the training set (Groups G1–G18) for hyperparameter tuning and model selection. This internal validation, detailed in the diagram, involves five folds where each subsequent blast event is predicted based on past data, preventing data leakage. The final model, trained on the entire training set (G1–G18), was evaluated on a strictly independent hold-out test set (G19–G23) to assess its generalizability

4 Model Application

Following the five rounds of fixed-step rolling cross-validation, the optimal hyperparameters for each coupled model were determined. These optimized parameters were then used to train the final models and generate predictions. The resulting optimal hyperparameter sets are summarized in Table 4.

Table 4: Table of optimal hyperparameters of the model

Predictive model	Key parameters	Optimization algorithm		
		CIPSO	GWO	MFO
SVR	Regularization parameter c	7.2041	30.9095	9.8384
	Gamma	0.001	0.4	0.01
	Epsilon	0.01	0.2752	0.01

(Continued)

Table 4 (continued)

Predictive model	Key parameters	Optimization algorithm		
		CIPSO	GWO	MFO
	η_1	0.01	0.05	0.02
CNN	FilterSize	2	4	5
	NumFilters	53	7	31
	η_2	0.04	0.1	0.06
LSTM	Number of hidden units	68	83	137
	Learning rate	0.0319	0.01	0.0256
	Dropout rate	0.32	0.45	0.44
	η_3	0.02	0.05	0.01

4.1 Model Evaluation

In this paper, six assessment metrics are used to evaluate and analyze the final prediction results, as shown below [34–36]:

$$R^2 = 1 - \frac{\sum_{i=1}^{m} (X_i - Y_i)^2}{\sum_{i=1}^{m} \left(X_i - \overline{X}\right)^2} \in [0.1] \tag{19}$$

$$MAE = \frac{1}{m} \sum_{i=1}^{m} |X_i - Y_i| \tag{20}$$

$$RMSE = \sqrt{\frac{1}{m} \times \sum_{i=1}^{m} (X_i - Y_i)^2} \tag{21}$$

$$d = 1 - \frac{\sum_{i=1}^{m} (X_i - Y_i)^2}{\sum_{i=1}^{m} \left[\left|X_i - \overline{X}\right| + \left|Y_i - \overline{Y}\right|\right]^2} \in [0,\ 1] \tag{22}$$

where m is the number of data points, X_i is the true value, Y_i is the predicted value, and $\overline{X}$ is the average of the true values

4.2 Performance Analysis of the Prediction Result Set

Fig. 10 presents the predicted vs. true value plots for the nine coupled models. A comparative performance analysis of these hybrid models is provided in Fig. 11.

As illustrated in Fig. 10, under the same optimization algorithm, the overall prediction trends of the SVR, CNN, and LSTM models align approximately with the measured values on both training and testing sets. Among them, the CIPSO-SVR model yields predictions that most closely match the true values. Fig. 11 further reveals that the CIPSO-SVR model demonstrates the most outstanding performance, achieving high R^2 values of 0.990 on the training set and 0.957 on the testing set. Its data

points cluster tightly around the y = x line and maintain strong consistency across the entire PPV range, indicating not only high overall accuracy but also stable predictive capability for blast vibrations of varying intensities. Notably, the three CIPSO-optimized models exhibit very few outliers significantly deviating from the y = x line. In contrast, models optimized by GWO and MFO, particularly those corresponding to subplots (e), (f), (h), and (i) in Fig. 11, display noticeable outlier points. The presence of these outliers, combined with the greater overall dispersion of the data, suggests a compromised generalization ability in these models.

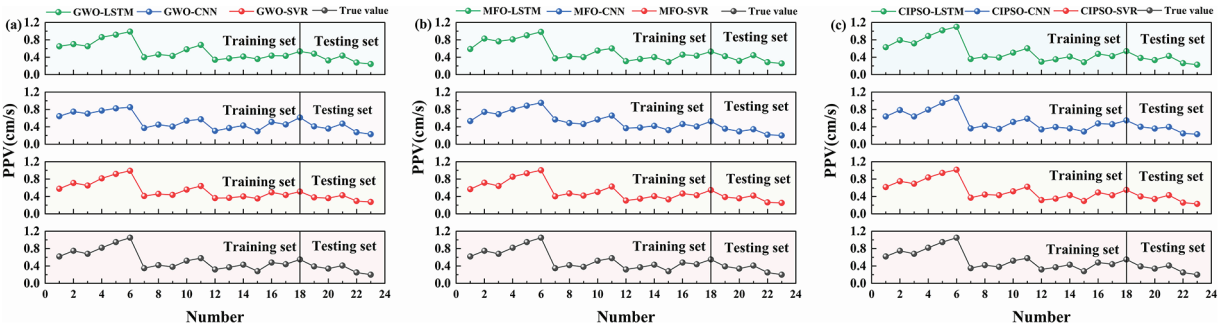

Figure 10: Comparison of predicted and measured PPV for the hybrid models: (**a**) corresponds to a comparison of predicted vs. measured values for the three models (LSTM, CNN, SVR) optimized by the GWO algorithm; (**b**) corresponds to a comparison of predicted vs. measured values for the three models (LSTM, CNN, SVR) optimized by the MFO algorithm; (**c**) corresponds to a comparison of predicted vs. measured values for the three models (LSTM, CNN, SVR) optimized by the CIPSO algorithm

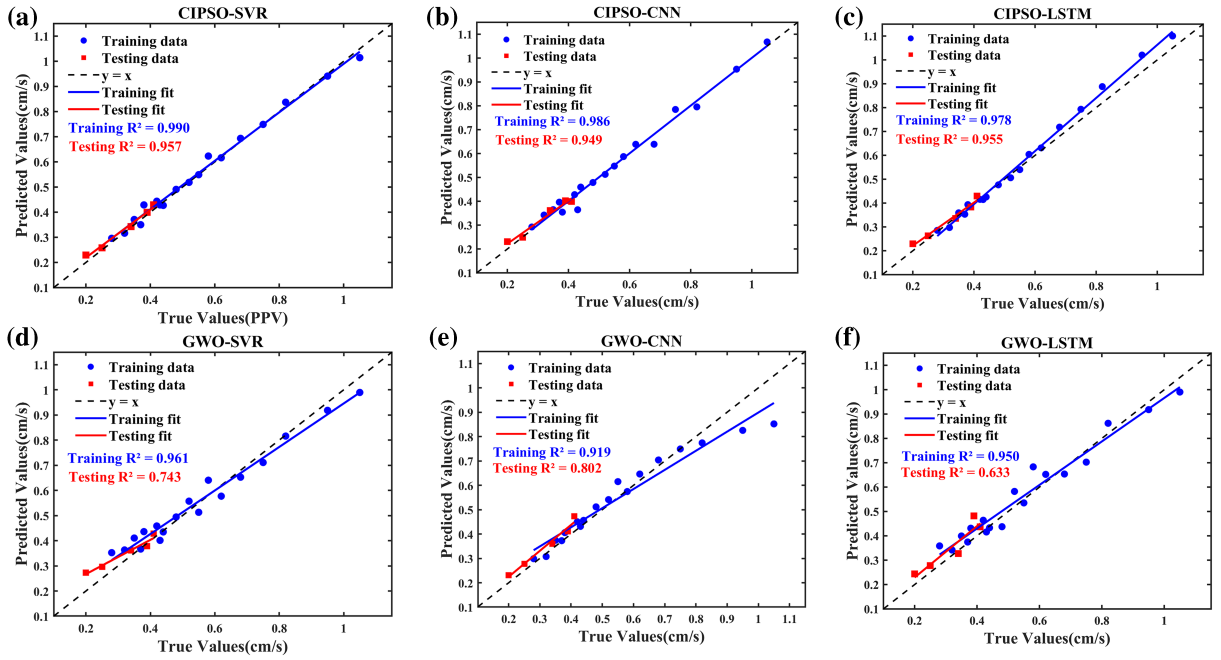

Figure 11: (Continued)

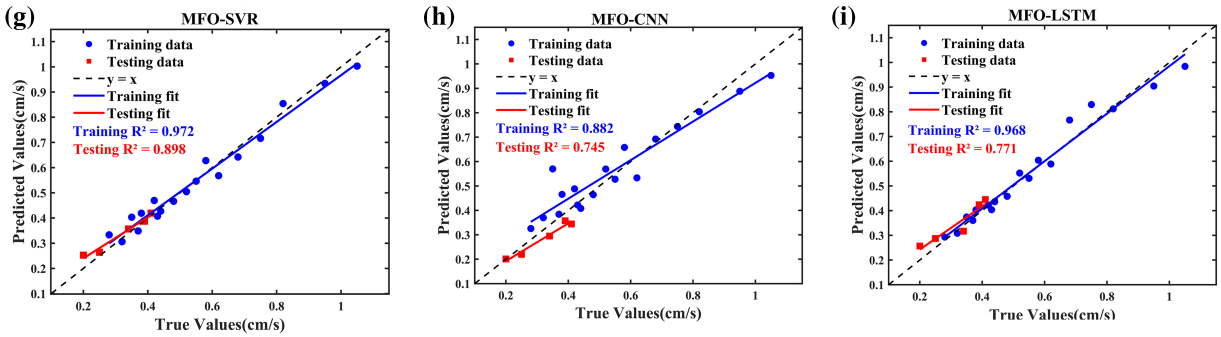

Figure 11: Scatter plots of predicted vs. measured PPV values for the nine hybrid models on both training and testing sets: (**a**) CIPSO-SVR; (**b**) CIPSO-CNN; (**c**) CIPSO-LSTM; (**d**) GWO-SVR; (**e**) GWO-CNN; (**f**) GWO-LSTM; (**g**) MFO-SVR; (**h**) MFO-CNN; (**i**) MFO-LSTM. The solid line represents the ideal fit (y = x). Models whose data points cluster tightly around this line exhibit higher accuracy. The CIPSO-SVR model (**a**) shows the closest agreement between predictions and measurements across both datasets, with minimal deviation from the ideal line, indicating its superior performance and generalizability

The integration of the Improved Particle Swarm Optimization (IPSO) algorithm with Support Vector Regression (SVR), further regularized by a physical constraint derived from Copula theory (the KL divergence term), establishes a robust framework for addressing tunnel blast vibration prediction under the challenges of small sample sizes and high nonlinearity. In contrast, while CNN and LSTM possess strong learning capabilities, their predictive performance diminishes in data-scarce scenarios. The comparative analysis confirms the superior efficacy of the CIPSO algorithm over GWO and MFO alternatives. These findings collectively demonstrate the enhanced capability of the proposed CIPSO-SVR approach in capturing complex nonlinear relationships within small-sample engineering contexts, offering a scientifically sound and effective predictive tool for analogous engineering problems.

To further analyze the prediction performance of the coupled models, the prediction errors ($PPV_{(\text{Predicted value-True value})}$) for each model are plotted in Fig. 12.

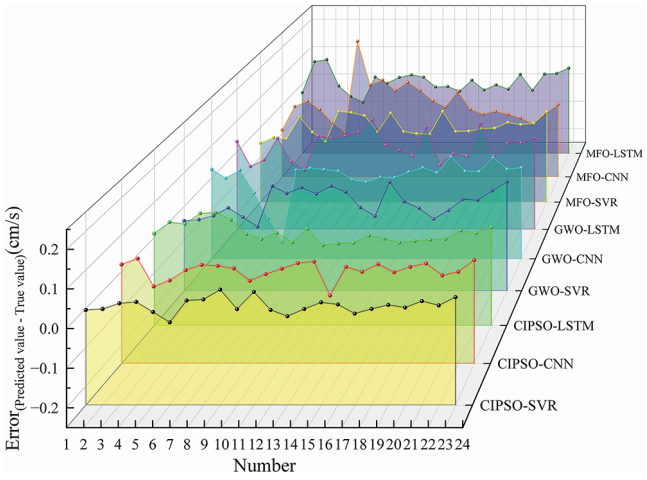

Figure 12: Error values for each coupled model

Fig. 12 demonstrates that the CIPSO-SVR model achieves superior accuracy compared to all other benchmark models (CIPSO-CNN, CIPSO-LSTM, GWO-SVR, GWO-CNN, GWO-LSTM, MFO-SVR, MFO-CNN, MFO-LSTM).

A comprehensive comparison of the error metrics for each coupled model is provided in Fig. 13 to further evaluate their prediction performance. In this figure, a larger R^2 value denotes a superior model fit, and a larger d indicates stronger consistency between predictions and measurements. Conversely, smaller values of both MAE and RMSE indicates lower prediction bias and higher overall accuracy, respectively.

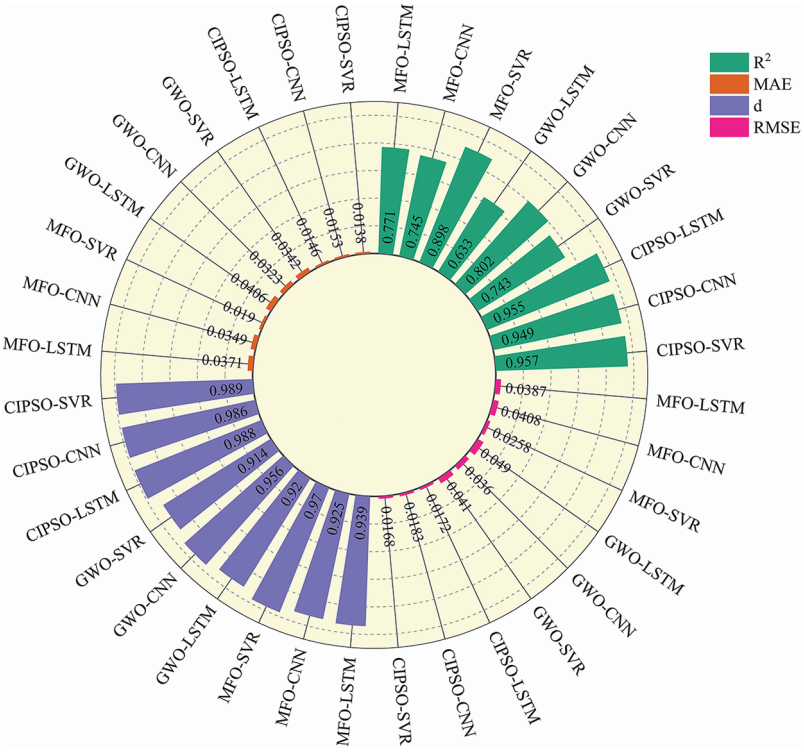

Figure 13: Error indicator plots for coupled models

Fig. 13 demonstrates that the SVR model optimized by the CIPSO algorithm achieves superior metrics (higher $R^2$and d, lower MAE and RMSE) compared to models optimized with the GWO and MFO algorithms. This confirms that CIPSO enhances both the model's fitting capability and its predictive accuracy. Among all nine coupled models, CIPSO-SVR delivers the best performance, with respective R^2, d, MAE, and RMSE values of 0.9569, 0.9888, 0.0138, and 0.0168, significantly outperforming the other eight models. These results affirm the high effectiveness of the proposed CIPSO-SVR model in solving complex nonlinear engineering problems.

The predictive performance of each coupled model on the test set, which can reflect solve real problems ability, is further evaluated using a Taylor diagram, as shown in Fig. 14.

As shown in the Fig. 14, the predictions of the CIPSO-SVR model are the closest to the measured data, followed by those of CIPSO-LSTM and CIPSO-CNN. This result demonstrates the superior practical performance of the CIPSO optimization algorithm compared to the GWO and MFO algorithms.

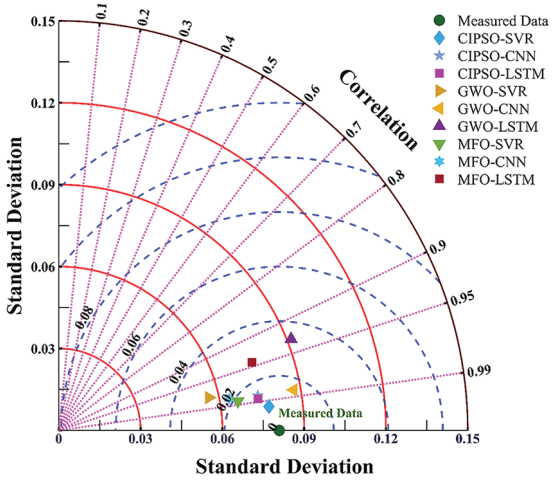

Figure 14: Taylor diagram visualizing the statistical agreement between predicted and measured PPV for each hybrid model on the test set. The proximity of a model's marker to the reference point ("Measured") on the diagram indicates the degree of similarity in terms of standard deviation, correlation coefficient, and centered RMS difference. The CIPSO-SVR model is located closest to the reference point, signifying the best overall statistical match to the observed data

4.3 Comparative Analysis of the CIPSO-SVR Model and Empirical Formulas for Prediction Performance

To further validate the practical contribution and engineering relevance of the proposed model, we compared its performance against the conventional empirical Sadovsky formula [37], which remains the most widely used method in blasting engineering practice for PPV prediction. The Sadovsky formula is expressed as:

$$PPV = k\left(\frac{\sqrt[3]{Q}}{R}\right)^{\alpha} \tag{23}$$

where PPV is the peak particle velocity (cm/s); R is the distance from the measuring point to the charge center (m); Q is the maximum amount of explosive detonated at one time (kg); k is a parameter related to the blasting site conditions; and α is a coefficient related to the geology.

$$\ln PPV = \ln k + \alpha \ln \frac{\sqrt[3]{Q}}{R} \tag{24}$$

Letting $Y = \ln PPV, b = \ln k, a = \alpha, X = \ln \frac{\sqrt[3]{Q}}{R}$, the above formula can be written as:

$$Y = b + aX \tag{25}$$

Fitting the training data using Eq. (12) yielded $b = 6.1921$ and $a = 2.2071$. Therefore, $\alpha = 2.2071$ and k = 488.8717. The Sadovsky formula is:

$$PPV = 488.8717\left(\frac{\sqrt[3]{Q}}{R}\right)^{2.2071} \tag{26}$$

The fitting results are shown in Fig. 15:

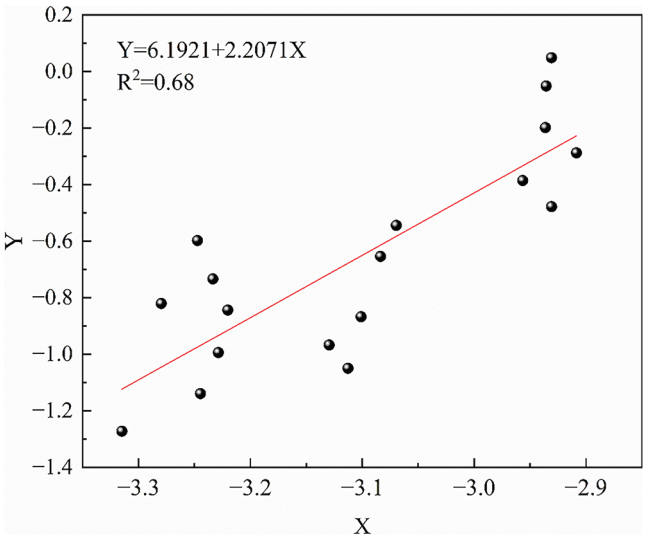

Figure 15: Linear regression fit of the Sadovsky equation on the training dataset

The test set was predicted using Eq. (26), and the results were compared with those from the CIPSO-SVR model. The performance of both approaches was evaluated using the mean absolute error (MAE), index of agreement (d) [38], root mean square error (RMSE), and Pearson correlation coefficient (PC), as summarized in Table 5.

Table 5: Comparison between the CIPSO-SVR model and the Sadovsky empirical formula

Prediction model	MAE	d	RMSE	PC
CIPSI-SVR	0.01382	0.98883	0.016779	0.99363
Sadovsky equation	0.040259	0.90341	0.048628	0.94661

As summarized in Table 5, the proposed CIPSO-SVR model demonstrates superior accuracy and consistency across all evaluated metrics compared to the Sadovsky empirical formula. Specifically, the CIPSO-SVR model achieved an index of agreement (d) of 0.98883 and a Pearson correlation coefficient (PC) of 0.9936, outperforming the empirical model, which yielded corresponding values of 0.90341 and 0.94661. This represents an improvement of 9.46% in predictive consistency and 4.97% in linear correlation. These results substantiate that the CIPSO-SVR model not only provides higher predictive accuracy but also yields results that are in closer agreement with physical reality. In contrast, the Sadovsky formula, owing to its simplistic form that considers only charge weight and distance, fails to capture the complex nonlinear interactions arising from varying geological conditions and blast design parameters. Furthermore, as a generalized model derived from broad empirical practice, it may lack the specificity required for optimal performance in particular engineering contexts.

4.4 Safety Control Interval Analysis and Engineering Decision Support Based on the CIPSO-SVR Model

To further elucidate the quantitative advantages of the CIPSO-SVR model for blasting safety decision-making, this section presents a safety control interval analysis. Unlike traditional empirical formulas, the proposed model outputs a full probability distribution for its predictions, enabling the construction of safety intervals and a formal risk assessment. Using 0.45 cm/s as the safety threshold, we conduct an in-depth analysis of the test set predictions, with the results presented in Fig. 16.

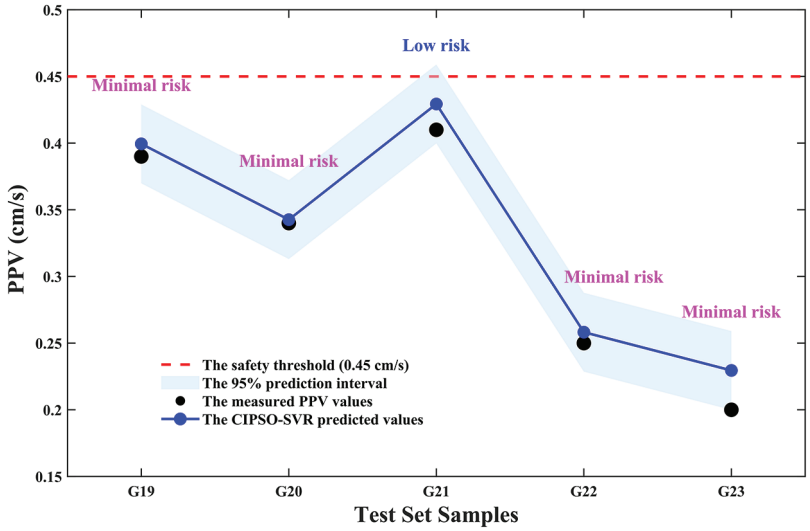

Figure 16: PPV Safety interval prediction and risk assessment based on the CIPSO-SVR model: The blue solid line represents the PPV values predicted by the CIPSO-SVR model, and the black dots denote the measured PPV values. The light blue shaded area depicts the 95% prediction interval, quantifying the uncertainty of the predictions. The red dashed line indicates the safety threshold of 0.45 cm/s. The safety threshold was established per the Chinese Blasting Safety Regulations (GB6722-2014), which stipulate a limit of 0.5 cm/s for the protection of ancient structures and historic sites. Given that the Ming Dynasty Great Wall is a National Key Cultural Relic, a more conservative threshold of 0.45 cm/s was adopted to ensure its maximum protection. The entire prediction interval lies consistently below the safety threshold, demonstrating a negligible risk of exceedance and providing a quantitative basis for safe blasting optimization

As shown in Fig. 16, the PPV values predicted by the CIPSO-SVR model closely align with the measured data, confirming its high predictive accuracy. The 95% prediction interval fully captures the variability in the measured values, while its upper boundary remains consistently below the safety threshold. Analysis indicates that the probability of the PPV exceeding the 0.45 cm/s safety threshold is extremely low, representing a negligible risk. This quantitative output provides a direct and reliable basis for optimizing blast designs. Supported by this evidence, engineers can safely adjust blasting parameters to improve efficiency, leading to significant savings in both project time and cost.

This study presents a hybrid prediction model, the Copula-theory-fused Improved Particle Swarm Optimization-based Support Vector Regression (CIPSO-SVR), for estimating peak particle velocity (PPV). The model incorporates the dependency structure characterized by the Copula function as a regularization term into the SVR objective function via the Kullback-Leibler (KL) divergence, thereby

enhancing prediction accuracy. Nevertheless, further refinements and optimizations of the proposed model are warranted.

Assumptions:

1) It is postulated that incorporating the Copula-derived dependency structure as a regularization term, via Kullback-Leibler (KL) divergence, into the Support Vector Regression (SVR) objective function can effectively guide the machine learning process. This integration is expected to steer predictions towards alignment with observed physical relationships, in addition to minimizing data-fitting errors, thereby potentially enhancing model generalizability under small-sample conditions.

2) The model training and cross-validation procedures operate under the assumption that data samples from individual blast events are independent and identically distributed. While the fixed-step rolling cross-validation method partially accounts for potential sequence dependence, the intrinsic dynamic time-series characteristics of vibration propagation are not explicitly modeled.

Limitations:

1) The model's development and evaluation are constrained by the dataset, which comprises only 23 valid samples obtained from the Jiao Shan Tunnel project. Its general applicability should be further tested across projects involving a broader range of geological settings.

2) Although the model demonstrates superior performance compared to other machine learning algorithms and empirical formulas within this study, a direct and systematic empirical comparison against established industry-standard methods in broader practical engineering.

Future Research Directions:

1) Future work will prioritize collecting blasting vibration data from a variety of tunnel projects and mining operations. Building a larger, more diverse dataset is crucial for a comprehensive assessment of the model's generalizability. Furthermore, Applying the proposed method to mining blasting scenarios will further test its applicability and robustness across different engineering environments.

2) Conducting parallel applications and comparative analyses alongside widely adopted empirical formulas and industry-standard software in future real-world projects is essential. Such comparisons will provide more compelling evidence regarding the model's practical value and effectiveness in engineering applications.

5 Conclusion

This study developed a novel blasting PPV prediction model by integrating Copula theory into an IPSO-SVR model framework, termed CIPSO-SVR. The core of this approach involves using a Copula function to quantify the correlation between PPV and surface settlement (S), which is then embedded as a physical constraint into the SVR objective function via KL divergence, ensuring the predictions adhere to engineering physics. This approach establishes the Copula theory-incorporated, termed the CIPSO-SVR blasting PPV prediction model. The proposed CIPSO-SVR model was validated using the Jiao Shan Tunnel project and compared against eight other machine learning methods. The principal conclusions are as follows:

1) Copula theory was successfully employed to quantify the nonlinear dependence between PPV and S. Based on the AIC/BIC criterion and tail dependence analysis, the Gumbel Copula function was identified as the optimal model for characterizing the PPV-S correlation at monitoring point D6 in section S1.

2) IPSO stabilizes the fitness function within 50 iterations, whereas PSO requires 60 iterations. The stabilized fitness value achieved by IPSO is lower, indicating faster convergence and higher solution accuracy when addressing complex nonlinear engineering problems.

3) On the test set, the proposed CIPSO-SVR model achieved superior performance metrics ($R^2 = 0.9569$, $d = 0.9888$, $MAE = 0.0138$ and $RMSE = 0.0168$) compared to the eight models. This result confirms the enhanced capability of the CIPSO-SVR model in solving complex nonlinear engineering problems.

Tunnel blasting construction is prone to safety accidents, which not only generate huge economic losses to society, but also bring injuries to the workers. Therefore it is necessary to predict the PPV generated by blasting. The results of this study show that it is feasible to analyze and predict using the CIPSO-SVR model.

The model can solve complex nonlinear engineering problems and provides a scientific basis for construction units to predict and control the impact of blasting vibration in advance.

Acknowledgement: Not applicable.

Funding Statement: The authors received no specific funding for this study.

Author Contributions: The authors confirm contribution to the paper as follows: Conceptualization, Yawen Cao, Rui Ma, Leifeng Zhang; methodology, Yawen Cao, Rui Ma, Leifeng Zhang; software, Rui Ma and Leifeng Zhang; validation, Yawen Cao and Leifeng Zhang; formal analysis, Xiaofei Du and Wenjin Liu; investigation, Yawen Cao, Xiaofei Du, Wenjin Liu and Qixiang Gao; resources, Yawen Cao, Rui Ma, Leifeng Zhang; writing—original draft preparation, Yawen Cao, Rui Ma and Leifeng Zhang; writing—review and editing, Yawen Cao, Rui Ma, Xiaofei Du, Wenjin Liu and Qixiang Gao; visualization, Wenjin Liu and Qixiang Gao; supervision, Xiaofei Du and Wenjin Liu; project administration, Xiaofei Du and Qixiang Gao; funding acquisition, Yawen Cao, Xiaofei Du, Wenjin Liu. All authors reviewed the results and approved the final version of the manuscript.

Availability of Data and Materials: The data that support the findings of this study are available from the corresponding author upon reasonable request.

Ethics Approval: Not applicable.

Conflicts of Interest: The authors declare no conflicts of interest to report regarding the present study.

References

1. Xu M, Li X, Xu K, Liu T, Zhang Y, Yang T. Influence of the spatial distribution of underground tunnel group on its blasting vibration response. Undergr Space. 2023;10:248–68. doi:10.1016/j.undsp.2022.10.006.
2. Yan Y, Guo J, Bao S, Fei H. Prediction of peak particle velocity using hybrid random forest approach. Sci Rep. 2024;14:30793. doi:10.1038/s41598-024-81218-z.
3. Wu J, Yu C, Li H, Ma Y, Wang C. Quantifying uncertainty in blast-induced vibration velocity accounting for spatial variability of rock masses. Int J Geomech. 2025;25:04025117. doi:10.1061/IJGNAI.GMENG-10222.
4. Rong K, Xu X, Wang H, Yang J. Predicting the blast-induced ground vibration with support vector regression optimized by five swarm algorithms. Earth Sci Inf. 2025;18:1–20. doi:10.1007/s12145-025-01923-9.

5. Shylaja G, Prashanth R. A systematic survey of hybrid ML techniques for predicting peak particle velocity (PPV) in open-cast mine blasting operations. Artif Intell Rev. 2025;58:203. doi:10.1007/s10462-025-11156-3.
6. Gu Z, Xiong X, Yang C, Cao M, Xu C. Research on prediction of PPV in open pit mine used on intelligent hybrid model of extreme gradient boosting. J Environ Manage. 2024;371:123248. doi:10.1016/j.jenvman.2024.123248.
7. Deng X, Wang J, Wang R, Liu Q. Influence of blasting vibrations generated by tunnel construction on an existing road. Int J Civ Eng. 2020;18:1381–93. doi:10.1007/s40999-020-00549-w.
8. Luo Y, Wei X, Huang J, Zhang G, Bian X, Li X. PPV distribution of sidewalls induced by underground cavern blasting excavation. Sci Rep. 2021;11:6647. doi:10.1038/s41598-021-86055-y.
9. Tribe J, Koroznikova L, Khandelwal M, Giri J. Evaluation and assessment of blast-induced ground vibrations in an underground gold mine: a case study. Nat Resour Res. 2021;30:4673–94. doi:10.1007/s11053-021-09943-0.
10. Chen Y, Long F, Kuang W, Zhang T. A method for predicting blast-induced ground vibration based on Mamdani Fuzzy Inference System. J Intell Fuzzy Syst. 2023;44:7513–22. doi:10.3233/JIFS-223195.
11. Ghasemi E, Kalhori H, Bagherpour R. A new hybrid ANFIS-PSO model for prediction of peak particle velocity due to bench blasting. Eng Comput. 2016;32:607–14. doi:10.1007/s00366-016-0438-1.
12. Wang J, Zhang L, Yang S, Lian S, Wang P, Yu L, et al. Optimized LSTM based on improved whale algorithm for surface subsidence deformation prediction. Electron Res Arch. 2023;31(6):3435–52. doi:10.3934/era.2023174.
13. Yang S, Yang Z, Zhang L, Guo Y, Wang J, Huang J. Research on deformation prediction of deep foundation pit excavation based on GWO-ELM model. Electron Res Arch. 2023;31,9(9):5685–700. doi:10.3934/era.2023288.
14. Huang Y, Zhou Z, Li M, Luo X. Prediction of ground vibration induced by rock blasting based on optimized support vector regression models. Comput Model Eng Sci. 2024;139:3147–65. doi:10.32604/cmes.2024.045947.
15. Ma T, Chen C, Shen L, Luo K, Jiang Z, Liu H, et al. A novel social network search and LightGBM framework for accurate prediction of blast-induced peak particle velocity. Front Struct Civil Eng. 2025;19:645–62. doi:10.1007/s11709-025-1166-7.
16. Yuan H, Zou Y, Li H, Ji S, Gu Z, He L, et al. Assessment of peak particle velocity of blast vibration using hybrid soft computing approaches. J Comput Des Eng. 2025;12:154–76. doi:10.1093/jcde/qwaf007.
17. Feiyu L, Yao Q, Maixia F. Prediction model for the stored-grain situation risk point based on broad learning network. IEEE Access. 2023;11:82037–49. doi:10.1109/ACCESS.2023.3300868.
18. Chesneau C. Theoretical validation of new two-dimensional one-variable-power copulas. Axioms. 2023;12:392. doi:10.3390/axioms12040392.
19. Bukovšek DK, Košir T, Mojškerc B, Omladič M. Non-exchangeability of copulas arising from shock models. J Comput Appl Math. 2019;358:61–83. doi:10.1016/j.cam.2019.02.031.
20. Sklar M. Fonctions de répartition à n dimensions et leurs marges. Paris, France: Publ Inst Stat Univ; 1959; p. 229–31. (In French).
21. Carvalho JH, Schwartz UB, Borges CLT. Copula based model for representation of hybrid power plants in non-sequential Monte Carlo reliability evaluation. Sustainable Energy Grids Netw. 2023;35:101077. doi:10.1016/j.segan.2023.101077.
22. Tankov P. Tails of weakly dependent random vectors. J Multivar Anal. 2016;145:73–86. doi:10.1016/j.jmva.2015.12.008.
23. Han L, Liu H, Zhang W, Wang L. A comprehensive comparison of copula models and multivariate normal distribution for geo-material parametric data. Comput Geotech. 2023;164:105777. doi:10.1016/j.compgeo.2023.105777.

24. Wang H, Yuan Y, Li Y, Wang X. Financial contagion and contagion channels in the forex market: a new approach via the dynamic mixture copula-extreme value theory. Econ Model. 2021;94:401–14. doi:10.1016/j.econmod.2020.10.002.
25. Ly S, Sarwat S, Wong WK, Ramzan M, Nguyen HD. A static and dynamic copula-based ARIMA-fGARCH approach to determinants of carbon dioxide emissions in Argentina. Environ Sci Pollut Res.. 2022;29:73241–61. doi:10.1007/s11356-022-20906-7.
26. Vapnik V, Golowich S, Smola A. Support vector method for function approximation, regression estimation and signal processing. Adv Neural Inf Process Syst. 1997;9:281–7.
27. Peng C, Che Z, Liao TW, Zhang Z. Prediction using multi-objective slime mould algorithm optimized support vector regression model. Appl Soft Comput. 2023;145:110580. doi:10.1016/j.asoc.2023.110580.
28. Bisoyi SK, Khatti J, Fissha Y, Behera B, Pal BK, Sazid M. Optimizing blast-induced vibration predictions using hybrid ANN: a study in Dongri-Buzurg mine. J Appl Geophys. 2025;241:105867. doi:10.1016/j.jappgeo.2025.105867.
29. Jin W, Guan S, Chen L, Tang Z, Huang M, Xu X, et al. Joint risk analysis of typhoon hazards based on coupled ADCIRC-SWAN model simulations around Hainan. China J Sea Res. 2025;205:102587. doi:10.1016/j.seares.2025.102587.
30. Wei Y, Xu ZD, Tao Y, He JX, Tian Y, Lu Y. Copula-based hazard analysis of office buildings exposed to potential earthquake-fire impacts. J Build Eng. 2025;100:111657. doi:10.1016/j.jobe.2024.111657.
31. Jacobs K, Jacobs K. Elements of information theory. In: Discrete stochastics. Basel, Switzerland: Birkhäuser; 1992. p. 155–83. doi:10.1007/978-3-0348-8645-1_7.
32. Chopra N, Brar YS, Dhillon JS. An improved particle swarm optimization using simplex-based deterministic approach for economic-emission power dispatch problem. Elect Eng. 2021;103:1347–65. doi:10.1007/s00202-020-01164-7.
33. Galeazzi A, Fusco FD, Manenti BF. Predicting the performance of an industrial furnace using Gaussian process and linear regression: a comparison. Comput Chem Eng. 2024;181:108513. doi:10.1016/j.compchemeng.2023.108513.
34. Gao F, Xie J, Xiong X, Wang L, Chang X. Prediction of peak particle vibration velocity based on intelligent optimization algorithm combined with XGBoost. Expert Syst Appl. 2025;280:127654. doi:10.1016/j.eswa.2025.127654.
35. Zhou J, Qiu Y, Khandelwal M, Zhu S, Zhang X. Developing a hybrid model of Jaya algorithm-based extreme gradient boosting machine to estimate blast-induced ground vibrations. Int J Rock Mech Min Sci. 2021;145:104856. doi:10.1016/j.ijrmms.2021.104856.
36. Abraham MT, Satyam N, Pradhan B, Tian H. Debris flow simulation 2D (DFS 2D): numerical modelling of debris flows and calibration of friction parameters. J Rock Mech Geotech Eng. 2022;14:1747–60. doi:10.1016/j.jrmge.2022.01.004.
37. Shan R, Zhao Y, Wang H, Dong J, Wang D. Research on the attenuation law of blasting vibration in tunnel engineering. Arab J Geosci. 2022;15:631. doi:10.1007/s12517-022-09899-2.
38. Hodson T. Root-mean-square error (RMSE) or mean absolute error (MAE): when to use them or not. Geosci Model Dev. 2022;15(14):5481–7. doi:10.5194/gmd-15-5481-2022.